Epitaxial alloyed films out of the bulk stability domain: Surface structure and composition of Ni₃Al and NiAl films on a stepped Ni(1 1 1) surface

G. Prévot [a,*], D. Schmaus [a,b], S. Le Moal [c,1]

[a] Institut des NanoSciences de Paris, UMR CNRS 7588, Université Pierre et Marie Curie-Paris 6, 140, rue de Lourmel, 75015 Paris, France
[b] Université Paris Diderot-Paris 7, 140, rue de Lourmel, 75015 Paris, France
[c] Lehrstuhl für Physikalische Chemie, Technische Universität München, Lichtenbergstrasse 4, 85747 Garching, Germany

ABSTRACT

We have studied by Spot Profile Analysis Low Energy Electron Diffraction (SPA-LEED) and Auger Electron Spectroscopy (AES) Ni–Al alloyed layers formed by annealing, around 780 K, Al deposits on a stepped Ni(1 1 1) surface. The surface structure and composition of the thin epitaxial Ni₃Al and NiAl films, obtained respectively below and above a critical Al initial coverage θ_c, differ markedly from those of corresponding bulk alloys.

The Ni₃Al ordered films form in a concentration range larger than the stability domain of the L1₂ Ni₃Al phase. The NiAl films present a marked distortion with respect to the lattice unit cell of the B2 NiAl phase, which slowly decreases when the film thickness increases.

It also appears that the value of θ_c depends on the morphology of the Ni(1 1 1) substrate, increasing from $\theta_c = 4.5$ ML for a flat surface to $\theta_c = 10$ ML for a surface with a miscut of 0.4°. This could be directly related to the presence of steps, which favour Ni–Al interdiffusion.

© 2010 Elsevier B.V. All rights reserved.

1. Introduction

Ni–Al alloys are of great technological interest because of their remarkable mechanical and thermal properties, namely a high hardness and high melting points. They are also resistant to corrosion, owing to the formation at their surface of a thin passive film of aluminium oxide acting as a diffusion barrier. For all these reasons, the use of these alloys is widely developed in aeronautics (turbo reactors) [1], in energy storage and furnace hardware, and in microelectronics (epitaxial contacts to III–V semiconductors, corrosion resistant metal coatings [2]). Moreover, ultrathin well-ordered Al₂O₃ layers can be obtained by oxidation at high temperature of Ni₃Al or NiAl single crystals [3]. Besides, two recent studies have reported the possibility to prepare such oxide films from the oxidation of thin Ni₃Al alloyed layers grown on Ni(1 0 0) or on Ni(1 1 1) [4,5]. These ultrathin epitaxial Al₂O₃ films have become increasingly attractive in catalysis as model-supports for epitaxy of small metallic aggregates [6] and in magnetism as insulating barrier in magnetic tunnel junctions [7].
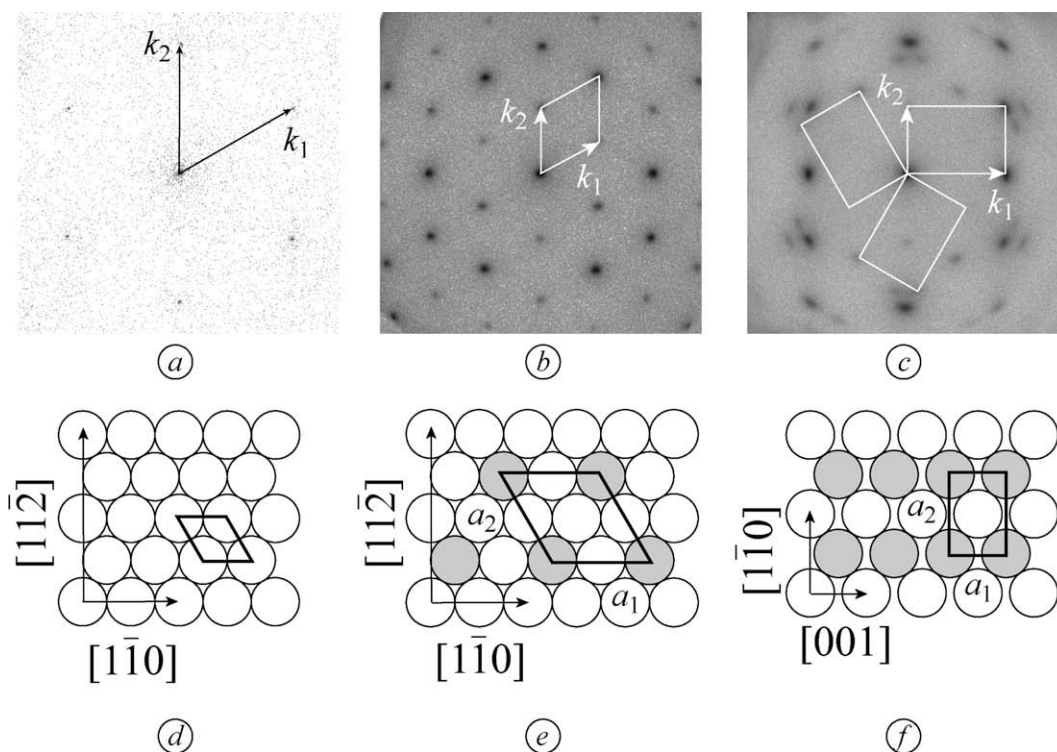
The phase diagram of the Ni–Al system reveals the existence of four ordered compounds, namely NiAl₃, Ni₂Al₃, NiAl and Ni₃Al [8]. In two previous studies [9,10], we have described the formation of the two richer phases in Ni upon annealing Al deposits on Ni(1 1 1), with a strong dependence on the nominal thickness of the initial Al layer. Below a critical thickness θ_c which was found to be $\theta_c \approx 4.5$ monolayers (ML), annealing around 750 K yields an ordered Ni₃Al layer in epitaxy with the Ni substrate, with Ni₃Al(1 1 1)∥Ni(1 1 1) and Ni₃Al [1 $\bar{1}$ 0]∥Ni[1 $\bar{1}$ 0] (see Fig. 1). This specific epitaxy is attributed to the fact that the fcc Ni and the cubic L1₂ Ni₃Al phase have very similar bulk lattice parameters ($a_0^{Ni} = 3.524$ Å and $a_0^{Ni_3Al} \approx 3.57$ Å). Above this critical thickness, annealing around 750 K leads to the formation of a crystalline cc B2 NiAl layer ($a_0^{NiAl} = 2.887$ Å) on top of an epitaxial Ni₃Al layer of constant thickness (18 (1 1 1) planes), in epitaxy with the underlying Ni₃Al layer, with the Nishiyama–Wasserman [11,12] epitaxial relationship, i.e. NiAl(1 1 0)∥Ni₃Al(1 1 1) and NiAl[0 0 1]∥Ni₃Al [1 $\bar{1}$ 0] (see Fig. 1). Due to the symmetry of the (1 1 1) Ni₃Al surface, three variants are possible for the in-plane orientation of NiAl. We have observed the formation of this NiAl layer up to thicknesses higher than 100 nm. Moreover, the critical thickness θ_c does not seem to depend on the annealing temperature in the 750–790 K temperature range [13], but annealing above 800 K results in a progressive dissolution of Al in the substrate.

Despite these two previous studies, some open questions remain. The origin of the transition between these two regimes is

* Corresponding author. Tel.: +33 1 44 27 46 53; fax: +33 1 43 54 28 78.
E-mail address: prevot@insp.jussieu.fr (G. Prévot).
[1] Present address: Centre Interdisciplinaire de Nanoscience de Marseille, CNRS - UPR 3118, Aix-Marseille Université Campus de Luminy, Case 913, 13288 Marseille Cedex 09, France.

Fig. 1. LEED patterns (primary energy 135 eV) of (a) bare Ni(1 1 1), (b) Ni$_3$Al(1 1 1) surface (obtained after annealing at 790 K of a 7 Al ML deposit on Ni(1 1 1)) and (c) NiAl(1 1 0) surface (obtained after annealing at 760 K of a 18 Al ML deposit on Ni(1 1 1)). In all cases the vectors (k_1 and k_2) of the surface unit cell ($p(1 \times 1)$ for Ni(1 1 1), $p(2 \times 2)$ for Ni$_3$Al(1 1 1) and three rectangular unit cells for NiAl(110)) are drawn on the LEED pattern. (d–f) Corresponding atomic arrangements in direct space, white and grey circles representing Ni and Al atoms, respectively. Please note that in (d–f) the surface unit cell is indicated by a black parallelogram with the surface lattice parameters a_1 and a_2. Vectors indexed with respect to the bulk unit cells are also drawn.

still unclear. It could either be related to the elastic energy stored in the Ni$_3$Al layer, the in-plane lattice parameter of the layer being 1% contracted in order to fit the Ni bulk lattice parameter [9], or to a kinetic transition during alloy formation by Ni–Al interdiffusion [14]. The origin of the Nishiyama–Wasserman epitaxial relationship is also unknown. As pointed out previously, there is a large misfit between the surface unit cells of Ni$_3$Al(1 1 1) and NiAl(1 1 0), but the corresponding interplanar distances only differ by 1% [10]. The fact that Ni$_3$Al(1 1 1) and NiAl(1 1 0) have the same step height could thus indicate that steps play a role in the transition. We wanted to characterise precisely the surface lattice parameters of the annealed films to determine if Ni$_3$Al(1 1 1) grows in registry with Ni(1 1 1), and whether NiAl(1 1 0) begin to growth in registry with Ni$_3$Al(1 1 1) at the transition, or not. For this purpose, we have precisely studied by Spot Profile Analysis Low Energy Electron Diffraction (SPA-LEED) and Auger Electron Spectroscopy (AES) the surface of the alloyed films obtained after annealing Al deposits on Ni(1 1 1) in a temperature range (760–790 K) very close to the one used in Refs. [9,10]. In order to underline the important role of steps in the alloying process we have used a stepped Ni(1 1 1) surface, with a miscut of 0.4°.

On this stepped surface, we recover the previous results concerning the transition, at a critical value θ_c, between Ni$_3$Al growth (for the "thinnest" Al deposits) and NiAl growth (for the "thickest" Al deposits). However, the transition occurs at a different value of θ_c, namely 10 ML, instead of 4.5 ML for a flat Ni surface [9,10]. In this paper, we show that this higher critical thickness observed for the transition could be directly related to the presence of steps, which favour Ni–Al interdiffusion. The experiments also reveal that the surface structure and composition of the alloyed films are quite different from those observed at the surface of the bulk phases at thermal equilibrium.

Our experimental set-up as well as the sample preparation are described in Section 2. A brief overview of the analysis procedure used for SPA-LEED and AES measurements is also presented in this part. The results obtained after low temperature deposition are presented in Section 3. Section 4 is devoted to the results obtained after annealing an initial Al deposit below the critical coverage θ_c, and Section 5, to the results obtained above θ_c. The last part of the paper is devoted to a discussion of the results, highlighting the crucial influence of steps on the interdiffusion processes, and to the conclusion.

2. Experimental

2.1. Set-up and sample preparation

The experiments have been performed in an UHV set-up (base pressure 10^{-10} Torr) equipped with facilities for preparing the sample, with a Omicron Spot Profile Analysis Low Energy Electron Diffractometer and a Riber Cylindrical Mirror Analyzer Auger Electron Spectrometer. The sample is hold by a high precision XYZ-$\theta\varphi$ manipulator; it can be heated up to 900 K and cooled down to 140 K.

The sample is a disk 9 mm in diameter and 3 mm in thickness, purchased from Surface Preparation Laboratory (Penningweg 69 F, 1507 DE Zaandam, The Netherlands). The crystal is miscut 0.4° from (1 1 1). The step density has been separately measured by Scanning Tunneling Microscopy: the mean terrace width is approximately equal to 300 Å, with steps running at 8 ± 5° from the [1 $\bar{1}$ 0] axis. Prior to experiments, the sample was cleaned by a series of cycles of Ar ion sputtering at 1 keV followed by annealing a few minutes at about 900 K. The cleanliness of the sample was checked

at the end of each cycle by AES, in particular by verifying the absence of carbon contamination.

Al is evaporated from a Mo crucible, using the Omicron EFM-3T evaporator. During Al evaporation, the sample is cooled down to 140 K in order to reduce the atomic mobility, which was previously assumed to avoid alloying during the deposition process [9,10]. The Al flux at the sample is controlled by monitoring the flux of evaporated ions on an electrode of the evaporator. The emission cone out of the evaporator yields a deposition area about 8 mm in diameter on the sample surface, and is put deliberately off centre of the Ni sample. Within the investigated conditions of growth, only the evaporation time is modified. All the other experimental parameters (Al flux, sample temperature, sample position with respect to the evaporator) are kept constant, within the experimental uncertainties. After evaporation, the sample is annealed for 20 min at temperatures between 760 K and 790 K. Before and after annealing, AES and SPA-LEED measurements are performed at several points of the sample. The electron beam is about 0.1 mm in diameter for AES, and 1 mm for SPA-LEED.

2.2. Coverage measurements

In this paper, we define the Al coverage θ as the ratio of the deposited Al density to the atomic density of a Ni(1 1 1) plane, that is: 1 ML = 1.86×10^{15} atoms/cm^2.

The Al quantities at various points of the sample have been measured twice in an absolute way by ex-situ Rutherford Backscattering Spectrometry (RBS), with a 2.5 MeV Van de Graaff Ion Accelerator at the Institut des NanoSciences de Paris. In order to minimize the signal due to the Ni substrate, the measurements were performed by using a relatively grazing detection geometry (detection at 15° or 25° from the surface) and axial channelling conditions, namely alignment of either the [1 1 1] or the [1 1 0] Ni axis with the well-collimated incident beam (for more details see [9,10]). With these RBS experiments, we have verified the reproducibility of the Al evaporation conditions within the range of experimental uncertainties, and obtained the absolute calibration of the Al flux on the sample. Due to the fact that the sample is not aligned with respect to the evaporator, the amount of deposited Al is nearly constant on half the sample, and varies linearly on the other half of the sample. The Al evaporation rate in the plateau region of the sample is equal to (9.7 ± 0.3) ML per hour. The overall uncertainty on the Al coverage can be estimated from the different contributions that have to be taken into account: the uncertainties on

– the absolute value of the RBS reference standard [9];
– the RBS measurements due to counting statistics;
– the flux monitoring during evaporation;
– the sample position with respect to the evaporator, to the LEED and AES apparatus.

The total uncertainty, obtained by summing the squares of the different uncorrelated uncertainties is ranging from ±3% in the plateau region up to ±7% in the low coverage region of the sample.

2.3. SPA-LEED measurements

In the whole paper, we note $\vec{k}_i$ and $\vec{k}_d$ the wave vector of the incoming and diffracted beams, with $k_i = k_d = 2\pi/\lambda$, where λ is the wavelength, and $\vec{k} = \vec{k}_d - \vec{k}_i$ is the diffracted wave vector. All results presented here have been obtained at room temperature, with 135 eV electrons. For Ni(1 1 1), such energy approximately corresponds to maxima of intensity for the (0, 0), (1, 0) and equivalent spots (in-phase condition), and to minima of intensity for the (0, 1) and equivalent spots (out of phase condition).

For obtaining information about the surface structures of the alloyed layers we have precisely measured the relative positions of the diffraction spots for the different coverages and annealing temperatures used. Informations obtained from the study of the width of the diffraction spots, in correlation with scanning tunneling microscopy observations will be the subject of a forthcoming paper.

The diffraction spots are indexed with respect to the surface unit cell of the corresponding films. For each phase, parameters a_1 and a_2 correspond to the dimensions of the surface unit cell in direct space, whereas parameters k_1 and k_2 correspond to the dimensions of the surface unit cell in reciprocal space (see Fig. 1). Table 1 lists the correspondence between the bulk lattice parameters and the dimensions of the surface unit cell of bulk-terminated Ni(1 1 1), Ni$_3$Al(1 1 1) and NiAl(1 1 0) surfaces.

Quantitative information about the surface lattice parameters has been obtained from the positions of the diffractions spots. For all Al deposits, a calibration of the SPA-LEED apparatus has been carefully performed on the bare Ni(1 1 1) prior to evaporation. This calibration is also necessary for correcting the small geometrical distortions due to the imperfections of the deflecting electrodes of the SPA-LEED apparatus. However, due to the fact that the SPA-LEED electron gun is shut down during evaporation and annealing, this calibration deserves to be checked after evaporation and annealing. Nevertheless, the calibration has been found to be almost the same in all experiments. From the variations of calibration observed on Ni(1 1 1), we estimate the lattice parameters to be experimentally measured to a precision of ±0.3%. Diffraction profiles were fitted by lorentzian shapes. For Ni$_3$Al, the whole set of diffraction spots up to the (2, 0) equivalent spots are taken into account. For NiAl, only the spots corresponding to the major variant have been measured.

2.4. AES measurements

Information about the surface composition has been derived from AES spectra, using the Ni$_{MVV}$ transition at 61 eV, the Al$_{LVV}$ transition at 68 eV (hereafter named Ni61 and Al68, respectively) and the Ni$_{LMM}$ transition at 848 eV. AES spectra were acquired using incident electrons at 1800 eV. The signal was detected through a lock-in amplifier working with a 1 kHz modulation of 0.4 V amplitude applied on the cylinder of the CMA. The AES signal $I(E)$ is obtained by derivating $N(E)$ where $N(E)$ is the electron current detected at an energy E: $I(E) = dN/dE$. In our set-up, this is done directly through the lock-in amplifier. The peak heights are measured in the same way as in Ref. [15]. The energy resolution of the apparatus is about 0.4 eV. We estimate that the uncertainties on AES peak heights are ±10%, and that the uncertainties on the peak ratios are ±14%.

For each experiment, AES measurements have been performed just after deposition at the deposition temperature (140 K) and after annealing, at room temperature. In the same way as for LEED measurements, we have measured the AES signals at various points of the sample, thus exploring zones with different coverages. The time for performing these measurements was typically 1 h. We never observed variations of the AES signals measured at

Table 1
Bulk lattice parameter a_0 of Ni, Ni$_3$Al and NiAl and surface lattice parameters a_1 and a_2 (see Fig. 1) of Ni(1 1 1), Ni$_3$Al(1 1 1) and NiAl(1 1 0), for bulk-terminated surfaces.

	a_0 (Å)	a_1 (Å)	a_2 (Å)	a_1/a_0	a_2/a_0
Ni(1 1 1)	3.524	2.492	2.492	$1/\sqrt{2}$	$1/\sqrt{2}$
Ni$_3$Al(1 1 1)	3.57	5.05	5.05	$\sqrt{2}$	$\sqrt{2}$
NiAl(1 1 0)	2.887	2.887	4.083	1	$\sqrt{2}$
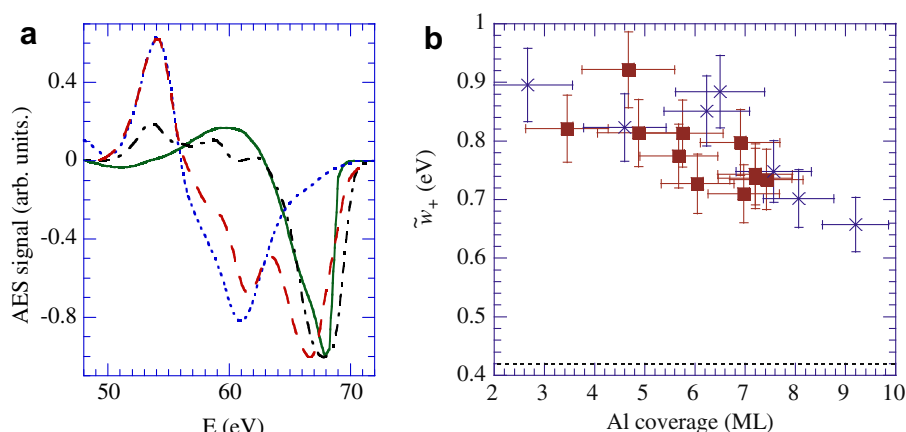
Fig. 2. a. AES low energy spectra of bare Ni(1 1 1) (blue dotted line), of 3.5 ML Al/Ni(1 1 1) (black dashed-dotted line) and of 30 ML Al/Ni(1 1 1) (continuous green line) just after deposition at 140 K, and of 18 ML Al/Ni(1 1 1) after annealing at 760 K (red dashed line). The normalization factor is not the same for each spectrum. b. Evolution of the width $\bar{w}_+^{Al}$ of the Al peak (see text) during deposition at 140 K as a function of the Al coverage θ. The dashed line indicates the width measured for $\theta = 20$ ML. The different symbols correspond to different experiments.

the same position on the sample either at the beginning or at the end of the procedure.

3. Surface of the films after deposition

As shown in Fig. 1a, the bare Ni(1 1 1) surface (before Al deposition) presents a very sharp (1 × 1) LEED pattern. After low temperature (140 K) deposition, the diffraction spots originating from Ni(1 1 1) progressively disappear with coverage, whereas very diffuse spots characteristic from an Al short range hexagonal ordering appear [9]. In this section, we focus on the results obtained by AES on the surface composition of the deposited layer.

3.1. Influence of alloying on the shape of the low energy AES spectra

AES low energy spectra of bare Ni(1 1 1) (blue[2] dotted line), of 3.5 ML Al (black dashed-dotted line), and of 30 ML Al (continuous green line) just after deposition at 140 K, are presented in Fig. 2a. For comparison, the AES spectrum obtained with a 18 ML Al/Ni(1 1 1) after annealing at 760 K (red dashed line) is also shown on Fig. 2a. The spectrum obtained for 30 ML Al at low temperature is similar to that obtained for a bulk Al. The spectrum registered for the 18 ML deposit annealed at 760 K is characteristic of the (1 1 0) surface of a thin NiAl alloyed film [10], and is also identical to that previously reported for NiAl(1 1 0) single crystal [16]. The comparison of these three low energy spectra shows that the spectrum of a NiAl alloy is not obtained by superimposition of the spectra of pure Ni and Al. In particular a shift of the peak position of the Al LVV transition towards lower energy is clearly visible, and the peak is wider. Such an effect is clearly visible for 3.5 ML Al deposited at 140 K. This indicates that the electronic structure of a 3.5 ML Al layer is not the same as the structure of bulk Al.

In order to go further, we have followed the shape of the Al peak during low temperature deposition. As can be seen in Fig. 2a, the Al peak at 68 eV is highly asymmetric, with a right part more abrupt than the left one. The minimum of the signal I_{min} is obtained at 68 eV, whereas the maximum of the derivative $(dI/dE)_{max}$ is obtained at 68.7 eV. We define the width of the right side of the Al peak as $\bar{w}_+ = -\frac{1}{2} \frac{I_{min}}{(dI/dE)_{max}}$. For bulk-like Al, $\bar{w}_+ = 0.42$ eV. The evolution of $\bar{w}_+$ with coverage is presented in Fig. 2b. Even for 10 ML coverage, we measure a value of $\bar{w}_+$ significantly higher

($\bar{w}_+ = 0.66$ eV) than for bulk-like Al. This is the signature that some Ni atoms are present in the near-surface Al layers, even for about ten ML deposited at 140 K, and modify the electronic properties of Al atoms.

### 3.2. Evolution with coverage of the surface composition during low temperature deposition

During deposition, we have also followed the evolution of the relative intensities of the Al and Ni peak. In particular, we present in Fig. 3a the Al68/Ni848 peak height ratio $r_{Al68/Ni848}$ measured just after deposition as a function of the Al coverage. We have used the SESSA software [17] for calculating the theoretical evolution of the AES intensities in absence of any alloying, taking into account our geometric configuration. We find that the intensity of Ni peaks should decay exponentially with coverage with a decay length of about 11 Å for Ni848 and about 1.5 Å for Ni61, whereas the intensity of Al peak at 68 eV would be almost constant above a thickness of 5 Å. In our case, using the definition of the coverage given in Section 2.2, 1 ML Al corresponds to an equivalent thickness of 3.09 Å for a bulk-like Al layer. Thus, for coverage higher than 1 ML, $r_{Al68/Ni848}$ should increase exponentially with a characteristic length of 3.6 ML. The experimental measurements of $r_{Al68/Ni848}$ also display an increase, but with a characteristic length of about 6.8 ML. Thus, for a 18 ML thick deposit, $r_{Al68/Ni848}$ is 10 times lower than expected for a pure Al layer of constant thickness. Such a difference could be due to roughness: parts of the sample covered with a smaller amount of Al would contribute to the Ni848 signal. However, if one assumes that the thickness distribution takes a gaussian form, the rms corresponding to the observed signal should be 20 ML. This roughness is much too high for a low temperature deposit.

We have tried to simulate these AES results, in a very rough approximation, assuming that the alloyed layer has a uniform thickness, and that the Ni concentration slowly decays in this layer. For doing this, we have made three assumptions:

- the variation of Ni concentration in the region probed by AES, near the surface, is small;
- the AES peak intensity depends linearly on the concentration and
- the chemical composition near the surface of a NiAl film obtained after annealing a 18 ML thick deposit is the stoichiometric composition since NiAl(1 1 0) has been found to have a

---

[2] For interpretation of color in Figs. 2–8, the reader is referred to the web version of this article.

a

b
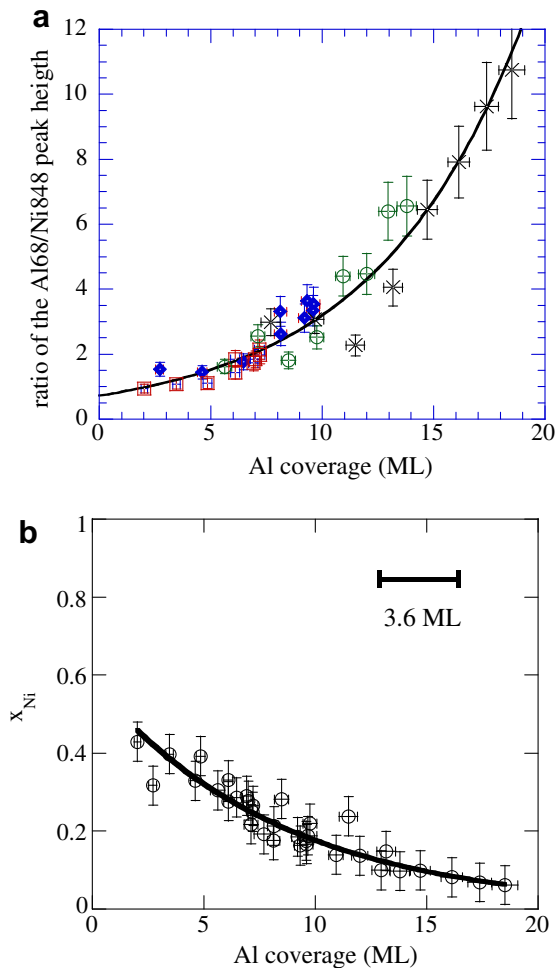
Fig. 3. a – Evolution of Al68/Ni848 AES peak heights ratio during deposition at 140 K as a function of Al coverage. The different symbols correspond to different deposits. The continuous line is an exponential fit $r = r_0 \exp(\theta/\theta_0)$ with $\theta_0 = 6.8$ ML. b – Evolution of the Ni atomic fraction x_{Ni} near the surface of the alloyed layer formed during deposition at 140 K, as a function of the Al coverage, deduced from the Al68/Ni848 peak height ratio. The horizontal bar indicates the attenuation length of 848 eV electrons in bulk Al (3.6 ML). The curve is a fit with $x = x_0 \exp(-\theta/\theta_0)$ with $\theta_0 = 8.3$ ML.

stoichiometric surface composition [18,19] and since our AES spectra for such layers are identical to those obtained on NiAl(1 1 0) [16]. Note that we do not take into account the fact that SPA-LEED measurements evidence a mean lattice parameter of the surface consistent with the bulk lattice parameter of $Ni_{0.60}Al_{0.40}$ (see Section 5.3).

In this model, $r_{Al68/Ni848}$ for a Ni_xAl_{1-x} layer can easily be deduced from the ratio $r_{Al68/Ni848} = 0.71$ measured on the $Ni_{50}Al_{50}$ surface. The evolution of the mean Ni atomic fraction x_{Ni} near the surface of the Al deposit is presented in Fig. 3b. It decays exponentially with a decay length of about 8.3 ML. Since it is much higher than the decay length of 3.6 ML for the attenuation of the AES signal of 848 eV electrons through a Al layer, this justifies our first approximation. If our third assumption is not correct, and if, for example, the composition near the surface of the NiAl layer obtained after annealing a 18 ML thick deposit is $Ni_{60}Al_{40}$, the value of x_{Ni} given in Fig. 3b has to be multiplied by 1.2.

The precise quantification of the alloy formation during deposition of Al/Ni is beyond the scope of this paper and requires measurement techniques sensitive to the chemical composition not only near the surface, but also in depth, for example medium energy ion scattering spectrometry (MEIS). However, we can conclude that on a sample with a high step density, like the one used in this study, Ni–Al interdiffusion at low temperature is higher than on a well oriented Ni(1 1 1) sample, for which no interdiffusion is observed at the same deposition temperature [9,10]. This leads to the presence of small amounts of Ni near the surface of the growing layer, even for Al deposits of about 20 ML.

4. Surface of Ni_3Al films after annealing

Below a critical coverage $\theta_c \approx 10$ ML, the structure corresponds to that of $Ni_3Al(1 1 1)$. New diffraction spots, related to the chemical order of Ni and Al atoms at the surface, appear on the LEED pattern (see Fig. 1). A typical SPA-LEED linescan is presented in Fig. 4. Diffraction spots have a lorentzian shape; apart from the diffraction spots mentioned, no other features are visible.
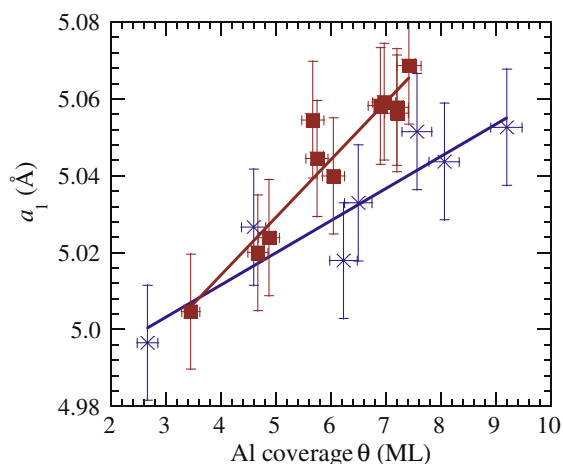
4.1. Surface lattice parameters of $Ni_3Al(1 1 1)$ after annealing

Fig. 5 plots the evolution of the lattice parameter $a_1 = a_2$ at the surface of the thin $Ni_3Al(1 1 1)$ film as a function of the coverage and for two different annealing temperatures. A general expansion of the surface lattice parameter with increasing θ is observed, namely from $a_1 \approx 5.00$ Å at $\theta \approx 2$ ML to $a_1 \approx 5.07$ Å at high coverage. The 1.5% variation observed is surprisingly large since the bulk lattice parameters of Ni and Ni_3Al, i.e. $a_0^{Ni} = 3.524$ Å and $a_0^{Ni_3Al} \approx 3.57$ Å, only differ by 1.3%. In our case, the lowest value of a_1 measured is close to twice the corresponding value for the (1 1 1) surface of a Ni crystal, i.e. 4.984 Å, whereas the highest value measured is close to the corresponding value for the (1 1 1) surface of a Ni_3Al crystal, i.e. 5.05 Å (see Table 1). As discussed below, this observation may provide information on the actual composition of the alloyed film, i.e. the atomic fraction of Al.

Lattice parameters ranging from $a_0^{Ni_3Al} \approx 3.556$ Å to $a_0^{Ni_3Al} \approx 3.584$ Å have been previously reported in the literature for bulk Ni_3Al, depending on the heat treatment and Al atomic fraction. Firstly, as reported in [20], the bulk lattice parameter of $Ni_{0.75}Al_{0.25}$ appears to depend on the heat treatment and cooling rate of the sample, with $a_0^{Ni_3Al} \approx 3.57 \pm 0.01$ Å. Secondly, for a given heat treatment and cooling rate, the bulk lattice parameter depends on the precise Al atomic fraction, inside the narrow stability domain (from $x_{Al} = 0.23$ to $x_{Al} = 0.275$) of the ordered $L1_2$ ordered $Ni_{1-x}Al_x$
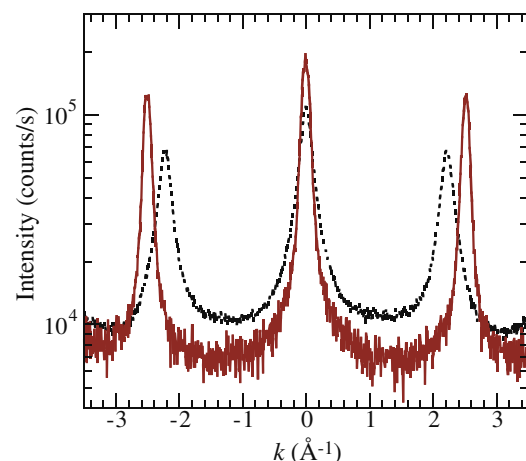
Fig. 4. SPA-LEED linescans on Ni_3Al and NiAl films, along the same direction $\vec{k}$, corresponding to $\vec{k}_1 - \vec{k}_2/2$ for $Ni_3Al(1 1 1)$ and to $\vec{k}_1$ for NiAl(1 1 0) (see Fig. 1). Continuous red line: Ni_3Al film obtained by annealing 7.4 ML Al at 790 K. Dotted black line: NiAl film obtained by annealing 11.1 ML Al at 760 K.

Fig. 5. Evolution of the surface lattice parameters $a_1 = a_2$ of the $Ni_3Al(1\,1\,1)$ film (see Fig. 1) as a function of Al coverage for different annealing temperatures T. Blue crosses: $T = 770$ K. Red squares: $T = 790$ K. Lines correspond to linear fits.

phase. Despite the discrepancies observed in the literature between the absolute values for a stoichiometric composition, it clearly appears that the lattice parameter of this bulk phase linearly increases with the Al atomic fraction, with a typical variation of 0.3% (see [21] for example) over the stability domain of this phase (i.e. for $\Delta x_{Al} = 0.045$). This effect is generally attributed to a much larger atomic radius for Al than for Ni. Remarkably, this rate of variation of $a_0^{Ni_3Al}$ with x_{Al} is rather consistent (in fact, larger by a factor 1.5) with the 1.3% variation of bulk lattice parameter between a_0^{Ni} and $a_0^{Ni_3Al}$ (for $\Delta x_{Al} = 0.25$).

Hence, it is surprising to observe such a large variation of the surface lattice parameters for this thin Ni_3Al films: the 1.5% variation of a_1 is about five times larger than the one foreseeable from [21]. This could be the signature that the $L1_2$ structure is stabilized, for the thin Ni_3Al film, in a larger Al concentration range than for the bulk compound at equilibrium. Assuming a linear variation of the bulk lattice parameter $a_0^{Ni_3Al}$ with x_{Al} [21], one can infer from our SPA-LEED measurements that the thin Ni_3Al films have an Al atomic fraction ranging from $x_{Al} = 10\%$ to $x_{Al} = 32\%$. Of course, this is a very rough approximation, since it assumes that the alloyed film keeps a "bulk-like" structure and it does not take into account any possible tetragonal distortion of the lattice. Moreover, let us recall that we measure the surface lattice parameters and not the bulk lattice parameters. It can be modified by the presence of steps that favours atomic relaxations in the surface plane that would not be allowed in the bulk.

4.2. Surface composition of Ni_3Al films after annealing

The evolution of the Al68/Ni848 and Al68/Ni61 peak height ratios, $r_{Al68/Ni848}$ and $r_{Al68/Ni61}$, after annealing the Al deposits at temperature between 760 K and 790 K, is presented in Fig. 6, as a function of the initial Al coverage θ. Since the attenuation length of the signal of 60–70 eV AES electrons is very small in our configuration (1.5 Å), the Al68 and Ni61 peaks are characteristic of the surface region, whereas the Ni848 signal takes into account the contribution of deeper layers (see above). However, the evolution of these ratios below θ_c is very surprising. They display a continuous evolution towards the signal corresponding to NiAl, whereas one should expect a plateau corresponding to the signal of a thick Ni_3Al layer. Both ratios display a similar evolution, as can be seen when comparing Fig. 6a and b. Here, we shall only comment Fig. 6b, representing $r_{Al68/Ni61}$. It increases only slowly between $\theta = 2$ ML and $\theta = 6$ ML, coverage at which it has a value equal to
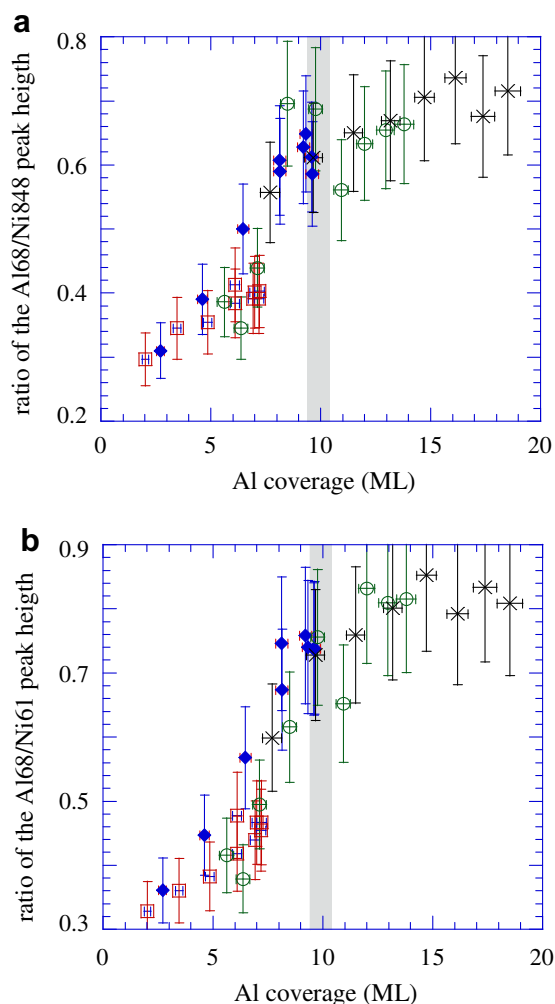

Fig. 6. Evolution of the Al68/Ni848 (a) and Al68/Ni61 (b) AES peak heights ratios as a function of Al coverage after annealing at high temperature. The annealing temperature are 760 K (crosses), 770 K (lozenges and circles), 790 K (squares).

0.4, whereas it increases markedly between $\theta = 6$ ML and $\theta = 10$ ML, up to a value around 0.8. Let us remark that for $\theta < 9.5$ ML, there is no LEED observation of a signal corresponding to NiAl domains at the surface. Noting that LEED is a technique sensitive to the organisation of small size domains, the evolution of the AES signal cannot be attributed to NiAl domains that would not be visible by electron diffraction. Even for small coverages, our AES spectra obtained on the annealed samples strongly differ from the spectra obtained on the (1 1 1) surface of a Ni_3Al single crystal. For such surface, $r_{Al68/Ni61} \approx 0.34$ [22], whereas the surface composition is still the same as in the bulk [23]. From this observation, we can infer that the Al atomic fraction at the surface of our Ni_3Al layer is always higher than $x_{Al} = 0.25$.

We have used the same procedure as in Section 3.2 for determining, from AES results, the Al concentration x_{Al} near the surface of the thin films grown. Note that with our simple model of linear variation of the Auger intensities with the atomic fraction, we should find a value $r_{Al68/Ni61} = 0.27$ for $Ni_3Al(1\,1\,1)$. However, for such small values of $r_{Al68/Ni61}$, the Al peak height could be overestimated, due to the presence of the shoulder of the Ni peak, and to the fact that the Al LVV transition is shifted towards lower energy due to alloying.

The values found by this procedure for x_{Al} are drawn in Fig. 7. In addition to these values derived from AES, we have drawn the values for x_{Al} that could be inferred from LEED measurements, by
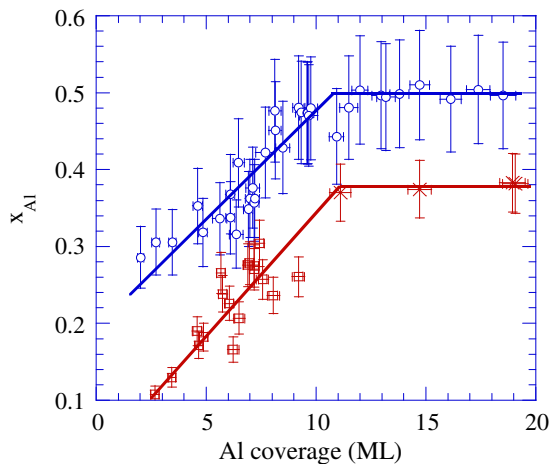
Fig. 7. Evolution of the Al atomic fraction x_{Al} near the surface of the thin films, obtained after annealing around 770 K an Al deposit, as a function of Al coverage. Blue circles: x_{Al} determined from AES measurements. Red symbols: x_{Al} determined from LEED measurements of the Ni$_3$Al surface lattice parameters (squares) and of the NiAl surface lattice parameters (crosses). Lines are guides for the eyes.

comparing the variation of the lattice parameters at the surface of the thin layer with the variation with composition of the lattice parameter of bulk alloys (see Section 4.2). The values of x_{Al} obtained by both procedures increase markedly with θ, up to $\theta_c \approx 10$ ML. This clearly confirms that the evolution of the surface lattice parameters measured for Ni$_3$Al films is related to an increase of the Al concentration at the surface. However the x_{Al} values inferred from SPA-LEED experiments are systematically lower by $\Delta x_{Al} \approx 0.12$ to 0.16 than those measured by AES. This indicates that the surface lattice parameters of Ni$_3$Al layers increases with Al concentration, but not exactly with the same factor as in the bulk.

5. Surface of NiAl films after annealing

5.1. Introduction

Above a critical coverage $\theta_c \approx 10$ ML, the structure corresponds to that of NiAl(1 1 0) with three variants. Typical diffraction pattern and SPA-LEED linescan are presented in Fig. 1c and Fig. 4. The orientation of NiAl(1 1 0) with respect to Ni(1 1 1), and to Ni$_3$Al(1 1 1) follows NiAl[0 0 1]‖Ni$_3$Al[1 $\bar{1}$ 0]‖Ni[1 $\bar{1}$ 0] and NiAl[1 $\bar{1}$ 0]‖Ni$_3$Al[1 1 $\bar{2}$]‖Ni[1 1 $\bar{2}$]. Note that in direct space, the smaller side a_1 of the NiAl(1 1 0) rectangular surface unit cell corresponds to NiAl[0 0 1]. Equivalent spots from the three variants of NiAl(1 1 0) do not have the same intensity, one variant giving rise to more intense spots than the two others, as can be seen in Fig. 1c. We ascribed the predominance of one of the variants to the specific orientation of the steps, since we found the major NiAl variant to have its [0 0 1] orientation almost parallel to the step edges.

We never simultaneously observe the diffraction patterns of the Ni$_3$Al(1 1 1) and NiAl(1 1 0) surfaces (see Fig. 1b and c, respectively) at the same position of the sample, except in a small region where $\theta \approx \theta_c$, i.e. where both areas with $\theta > \theta_c$ and $\theta < \theta_c$ are probed due to the finite size of the electron beam. These observations indicate a sharp lateral interface at the sample surface between a Ni$_3$Al(1 1 1) domain ($\theta \langle \theta_c$) and a NiAl(1 1 0) domain ($\theta \rangle \theta_c$). Let us remark that even in the close vicinity of the transition (around $\theta \approx 10$ ML), the diffraction spots corresponding to NiAl(1 1 0) could clearly be distinguished from those corresponding to Ni$_3$Al(1 1 1). It is possible that the transition at θ_c is from Ni$_3$Al/Ni(1 1 1) to NiAl/Ni$_3$Al/Ni(1 1 1) with a thinner Ni$_3$Al film. However we have previously shown by RBS investigations [10] that the NiAl(1 1 0)

film actually forms onto a Ni$_3$Al(1 1 1) interfacial layer whose Al content corresponds to θ_c. This could only be evidenced by RBS due to the subsurface sensitivity of this method, whereas LEED mainly probes the first surface plane. This shows that the variation of thickness of Ni$_3$Al at the transition, if any, is very small. In our case, for $\theta = 11$ ML, assuming that the Ni$_3$Al thickness is equal to 40 atomic planes, the thickness of the NiAl film observed should be equal to 2 atomic planes. Very thin NiAl films can thus be observed on Ni$_3$Al/Ni(1 1 1).

5.2. Lattice distortion at the surface of the NiAl film

In Fig. 8, we present separately, as a function of Al coverage, the evolution of the surface lattice parameters a_1 and a_2 of the NiAl(1 1 0) film (see Fig. 1 for the definition of a_1 and a_2). As compared to the (1 1 0) surface unit cell of a bulk NiAl crystal (see Table 1), the surface unit cell of the thin NiAl(1 1 0) film presents a significative distorsion, i.e. $a_1 < a_2/\sqrt{2}$. The variations of a_1 and a_2 with θ follow opposite trends: a_1 expands with increasing coverage, whereas a_2 contracts.

The ratio $r^{film} = a_2/\sqrt{2}a_1$, that measures the distortion of the rectangular cell at the surface with respect to its value for bulk alloys, has its maximum value ($r^{film} = 1.023$) near the transition and decreases down to ($r^{film} = 1.012$) for $\theta \approx 19$ ML. An extrapolation of our data for infinite thickness would lead to $r^{film} = 1$, that is a "bulk-like" rectangular unit cell of NiAl. In an attempt to explain the distortion of the thin NiAl(1 1 0) film, one may remark that this behaviour is qualitatively consistent with an accommodation with the underlying Ni$_3$Al(1 1 1) layer. However, the observed distortion is much too small to verify this model quantitatively. We discuss this argument more in details below.

The epitaxial relationship is NiAl[0 0 1]‖Ni$_3$Al [1 $\bar{1}$ 0] and NiAl [1 $\bar{1}$ 0]‖Ni$_3$Al[1 1 $\bar{2}$] (see Fig. 1e and f). The experimental values of a_1, reported in Fig. 8, appear to be markedly larger than the interatomic distance (2.52 Å $= a_0^{Ni_3Al}/\sqrt{2}$) along [1 $\bar{1}$ 0] at the (1 1 1) surface of a Ni$_3$Al crystal. This is visible in Fig. 4 where the same linescans performed on the Ni$_3$Al and NiAl surface are superimposed. The diffraction peaks of the two surfaces are clearly not at the same position. Conversely, the experimental values of a_2 appear to be smaller than the distance between two consecutive
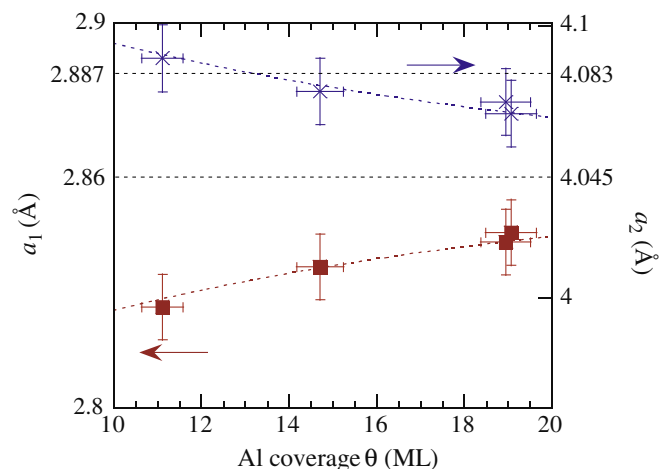
Fig. 8. Evolution of the size and shape of the rectangular surface unit cell for the NiAl(1 1 0) film as a function of Al coverage for an annealing temperature $T = 760$ K. The left and right scales differ by a factor of $\sqrt{2}$. Red squares correspond to a_1 and blue crosses correspond to a_2 (see Fig. 1). The blue and red dotted lines correspond to a global fit of the two curves with $a_1 = 2.86 - 0.035\exp(-(\theta - \theta_c)/12)$ and $a_2 = \sqrt{2}(2.86 + 0.035\exp(-(\theta - \theta_c)/12))$. The mean lattice parameter $\bar{a}_{surf} = a_1/2 + a_2/\sqrt{8} = 2.86$ Å and the NiAl bulk lattice parameter $a_0^{NiAl} = 2.887$ Å are also indicated.

$[1\bar{1}0]$ mixed Ni–Al rows at the (1 1 1) surface of a Ni₃Al crystal $(4.37\,\text{Å} = a_0^{\text{Ni}_3\text{Al}}\sqrt{3/2})$.

For a NiAl layer in registry with the underlying Ni₃Al film, one should thus obtain $r^{\text{film}} = \sqrt{3/2} \approx 1.225$. Our maximum value $r^{\text{film}} = 1.023$ measured by SPA-LEED reveals a distortion in the same way as for a pseudomorphic NiAl(1 1 0) rectangular cell, but one order of magnitude smaller. At this stage, one can conclude that the origin of the Nishiyama–Wasserman epitaxial relationship between NiAl and Ni₃Al is unknown and that since the misfit between the in-plane lattice parameters is much too high, the two structures are never in registry, even for coverage just above θ_c, for which the obtained NiAl layers are very thin.

5.3. Mean lattice parameter at the surface of the NiAl(1 1 0) film

In the following, we try to go further by examining the absolute values that we obtained for the lattice parameters of the NiAl(1 1 0) films and comparing them to bulk values.

The NiAl bulk lattice parameter $a_0^{\text{NiAl}} = 2.887\,\text{Å}$ is only valid for an atomic fraction of Al equal to $x_{\text{Al}} = 0.5$. In fact, the lattice parameter of bulk NiAl is known, since a long time, to vary markedly with x_{Al} all over the domain of existence (from $x_{\text{Al}} = 0.40$ to $x_{\text{Al}} = 0.56$) of the cubic B2 NiAl phase. Similarly to the case of L1₂ Ni₃Al (see sub-Section 4.1), this behaviour is due to a much larger atomic radius for Al than for Ni. However, the lattice parameter depends on x_{Al} in a more complicated way and the amplitude of the variation of a_0^{NiAl} is larger for NiAl [24,25]. For increasing values of x_{Al}, the lattice parameter of NiAl first increases from $a_0^{\text{NiAl}} = 2.865\,\text{Å}$ (for $x_{\text{Al}} = 0.40$) to a maximum value $a_0^{\text{NiAl}} = 2.887\,\text{Å}$ (for $x_{\text{Al}} = 0.5$) and then decreases down to $a_0^{\text{NiAl}} = 2.861\,\text{Å}$ (for $x_{\text{Al}} = 0.56$). The "paradoxical" decrease of a_0^{NiAl} when x_{Al} exceeds 0.5, in the "Al rich" side of domain of existence of the B2 phase, is attributed to Ni vacancies in the Ni sublattice (it is impossible to have two Al atoms as nearest neighbours in the cc B2 phase [26]).

Remarkably, the "mean" lattice parameter $\bar{a}_{\text{surf}} = (a_1/2 + a_2/\sqrt{8})$ of the NiAl films, averaged over both sides of the rectangular surface unit cell, is almost independent of θ and equal to 2.86 Å. This is shown in Fig. 8 by the qualitative fit with an opposite exponential decay for the two values: $a_1(\theta) = \bar{a}_{\text{surf}} + \Delta a \exp(-(\theta - \theta_c)/\Delta\theta)$ and $a_2(\theta) = \sqrt{2}(\bar{a}_{\text{surf}} - \Delta a \exp(-(\theta - \theta_c)/\Delta\theta))$ with $\Delta a = 0.035\,\text{Å}$, $\theta_c = 10$ ML and $\Delta\theta = 12$ ML. It can be noticed that this value $\bar{a}_{\text{surf}} = 2.86\,\text{Å}$ is smaller than that reported in the literature for a bulk-like stoichiometric NiAl but rather corresponds to the a_0^{NiAl} values reported for $x_{\text{Al}} = 0.40$ or $x_{\text{Al}} = 0.55$. This could indicate that, at the surface of the Ni–Al film, the Al atomic fraction could be either $x_{\text{Al}} = 0.40$ or $x_{\text{Al}} = 0.55$, both corresponding to the same value of $\bar{a}_{\text{surf}}$. It is then tempting to favour the value $x_{\text{Al}} = 0.40$, by continuity with the extremely high values of $x_{\text{Al}} = 0.32$ at the surface of the Ni₃Al(1 1 1) film deduced from our measurements of $\bar{a}_{\text{surf}}$ for $\theta \approx 10$ ML (see Subsection 4.2). In this model, the Al atomic fraction near the surface would not present a marked discontinuity at the transition. For Ni₃Al layers, it would increase with coverage, whereas for NiAl layer, it remains constant. This would explain why the mean surface lattice parameter of the NiAl film $\bar{a}_{\text{surf}}$ is independent of the thickness of the NiAl film. However the distortion of the surface NiAl lattice, induced by the underlying Ni₃Al(1 1 1) layer, decreases when the NiAl film thickness increases, and disappears only for thick deposits.

5.4. Surface composition of NiAl films after annealing

The evolution of the Al68/Ni848 and Al68/Ni61 peak height ratios, $r_{\text{Al68/Ni848}}$ and $r_{\text{Al68/Ni61}}$, after annealing the Al deposits at temperature between 760 K and 790 K, are also presented in Fig. 6, as a function of the initial Al coverage θ. For coverage $\theta > \theta_C \approx 10$ ML, these ratios are practically constant and correspond to that previ-

ously obtained for thick NiAl layers [10]. In Fig. 7, the comparison with surface composition determined from the mean surface lattice parameter of NiAl and from Auger measurements shows the same discrepancy for NiAl as for Ni₃Al: the x_{Al} values inferred from SPA-LEED experiments are lower by $\Delta x_{\text{Al}} \approx 0.12$ than the one measured by AES.

6. Discussion and conclusions

6.1. Thin Ni₃Al films with structure and composition very different from bulk alloys

The composition and lattice parameters at the surface of Ni₃Al films strongly differ from what should be expected for the (1 1 1) surface of a Ni₃Al stoichiometric crystal. It is first surprising to observe an ordered Ni₃Al layer with a surface Al concentration much higher than the upper limit of the stability domain of this phase $(0.23 < x_{\text{Al}} < 0.275)$. If we cannot exclude that the Al concentration is higher at the surface than in the bulk of the layer, the Al concentration must be different from $x_{\text{Al}} = 0.25$ in the bulk of the layer, since, as already mentioned, no surface segregation is observed for a stoichiometric Ni₃Al(1 1 1) [23]. Moreover, it would be very surprising to obtain a huge variation (of 1.5%) of the surface lattice parameter without any change of the lattice parameters in the bulk of the film. Our experiments show that it is possible to form Ni₃Al films in a concentration range very different from the bulk domain of stability. This allows us to interpret differently the results obtained by Tarento and Blaise in their study of the dissolution of Al on Ni [14].

They have measured concentration profiles obtained after annealing thick (200 nm) Al deposits on Ni(1 0 0). Different concentration plateaus have been observed after annealing a few hours at 500 K. For increasing annealing time, only the plateaus corresponding to lower Al contents are present. For example, after 11 h annealing at 500 K, plateaus at Ni₀.₄₄Al₀.₅₆, Ni₀.₆₀Al₀.₄₀ and Ni₀.₇₅Al₀.₂₅ are observed. Ni₀.₄₄Al₀.₅₆ and Ni₀.₆₀Al₀.₄₀ correspond to the limit of the stability domain of NiAl. The concentration profiles present a gap between $x_{\text{Al}} = 0.07$ and $x_{\text{Al}} = 0.23$, a region where no ordered compound is known to exist at thermal equilibrium [8]. However, in the similar region between $x_{\text{Al}} = 0.275$ and $x_{\text{Al}} = 0.40$, the concentration profile presents a smooth profile. This was attributed to a heterogeneous nucleation of NiAl and Ni₃Al in this region. From our study, it seems that it must be attributed to a non-stoichiometric Ni₃Al film.

Our study shows that using specific epitaxial conditions, thin crystalline Ni₃Al films can be stabilized over a much larger concentration range than bulk Ni₃Al. This opens very interesting perspectives, for example in the field of magnetism.

6.2. Role of the steps

Two observations demonstrate that steps have a marked influence on the growth of alloyed layers:

- the critical thickness θ_c is equal to 10 ML for a stepped (1 1 1) surface with a miscut of 0.4°, whereas θ_c is equal to 4.5 ML for a flat (1 1 1) surface with a miscut less than 0.1° [10] and
- on a (1 1 1) surface presenting a high step density, Ni diffusion in the Al layer occurs during deposition at 140 K, contrary to what is observed for a well oriented surface [9];

Since the Ni tracer diffusion coefficients in Al are several orders of magnitude larger than the Al tracer diffusion coefficients in Ni [27], diffusion of Ni through the growing layer occurs more rapidly than diffusion of Al in the Ni crystal. This is also in agreement with

our previous observations of a rapid diffusion of Ni at the surface of the Al layer during annealing at 750 K [10]. A possible origin for the formation of the alloyed layer would be the diffusion of Ni atoms in Al and in Ni_3Al from step sites. Ni atoms at these sites are less coordinated to other Ni atoms. In the early stage of alloying, such atoms could easily diffuse from the step edges into the Al layer. Since Ni_3Al grows epitaxially on Ni(1 1 1), its interface with NiAl will present the same atomic steps as the initial Ni(1 1 1) surface, leading to a higher interdiffusion of the species. This could also explain the increase of the critical thickness θ_c with the step density.

Steps could also favour the growth of thicker Ni_3Al films through the relieve of elastic energy. This is corroborated by the fact that Ni_3Al presents a surface atomic composition out of the domain of existence of the ordered $L1_2$ phase at thermal equilibrium, and surface lattice parameters very different from that could be expected from bulk Ni_3Al.

Finally, let us mention that the specific Nishiyama-Wasserman epitaxial relation observed for NiAl(1 1 0)/Ni_3Al(1 1 1) could also be due to the steps. The fact the Ni_3Al(1 1 1) and NiAl(1 1 0) surfaces have very similar interplanar distances (respectively 2.04 Å and 2.06 Å) could favour this epitaxy, in the case where NiAl domains begin to grow near the steps of Ni_3Al.

6.3. Conclusion

The formation of Ni–Al alloys by annealing Al deposits on Ni(1 1 1) depends on the morphology of the initial Ni surface. We have found that the critical thickness between the growth of Ni_3Al and the growth of NiAl increases from $\theta_c = 4.5$ ML for a surface with a miscut lower than 0.1°, to $\theta_c = 10$ ML for a surface with a miscut of 0.4°.

We have shown that these alloyed layers have a surface structure and composition very different from those of corresponding bulk alloys. For Ni_3Al, the surface lattice parameter increases with the Al coverage, in relation with a strong increase of the Al atomic fraction at the surface. In particular, we have evidenced an ordered Ni_3Al layer with a surface Al concentration x_{Al} close to 0.4–0.5, a value which is much higher than the upper limit of the bulk stability domain of this phase ($0.23 < x_{Al} < 0.275$). For NiAl layers, the surface presents a distortion with respect to the lattice unit cell of bulk NiAl. The amplitude of this distortion (2.3% for thin films) decreases when the Al coverage increases. The Al atomic fraction at the surface of such layers is constant, and close to $x_{Al} = 0.5$. Such Ni_3Al and NiAl layers could exhibit electronic and magnetic properties very different from the ones that could be inferred from the structure of the bulk alloy phases.

References

[1] D.B. Miracle, Acta Metall. 41 (1993) 649.
[2] P. Hannu, P. Kattelus, M.A. Nicolet, in: D. Gupta, P.S. Ho (Eds.), Diffusion Phenomena in Thin Films and Microelectronic Materials, Noyes publications, Park Ridge, NJ, 1988, p. 432.
[3] R. Franchy, Surf. Sci. Rep. 38 (2000) 195.
[4] A. Wehner, Y. Jeliazova, R. Franchy, Surf. Sci. 531 (2003) 287.
[5] S. Le Pévédic, D. Schmaus, C. Cohen, Surf. Sci. 602 (2008) 67.
[6] C. Becker, A. Rosenhahn, A. Wiltner, K. von Bergmann, J. Schneider, P. Pervan, M. Milun, M. Kralj, K. Wandelt, New. J. Phys. 4 (2002) 75.
[7] J.S. Moodera, L.R. Kinder, J. Appl. Phys. 79 (1996) 4724.
[8] M. Hansen, K. Anderko, Constitution of Binary Alloys, 2nd ed., Genium, New York, 1985, p. 119.
[9] S. Le Pévédic, D. Schmaus, C. Cohen, Surf. Sci. 600 (2006) 565.
[10] S. Le Pévédic, D. Schmaus, C. Cohen, Surf. Sci. 601 (2007) 395.
[11] Z. Nishiyama, Sci. Repts. Tohoku Imp. Univ. Tokio 23 (1934) 637.
[12] G. Wassermann, Mitt. K. – Wilh. – Inst. Eisenforsch. 17 (1935) 149.
[13] S. Le Pévédic, PhD Thesis, University Pierre et Marie Curie-Paris 6, Paris, 2007.
[14] R.J. Tarento, G. Blaise, Acta Metall. 37 (1989) 2305.
[15] A. Arranz, C. Palacio, Thin Solid Films 317 (1998) 55.
[16] H. Isern, G.S. Castro, Surf. Sci. 211/212 (1989) 865.
[17] W.S.M. Werner, W. Smekal, C.J. Powell, NIST database for the simulation of electron spectra for surface analysis, SRD 100, Version 1.0, National Institute of Standards and Technology, Gaithersburg, MD, 2005.
[18] D.R. Mullins, S.H. Overbury, Surf. Sci. 199 (1988) 141.
[19] X. Torrelles, F. Wendler, O. Bikondoa, H. Isern, W. Moritz, G.R. Castro, Surf. Sci. 487 (2001) 97.
[20] P.V. Mohan Rao, K. Satyanarayana Murthy, S.V. Suryanarayana, S.V. Nagender Naidu, Phys. Stat. Sol. (a) 133 (1992) 231.
[21] O. Noguchi, Y. Pia, T. Suzuki, Metal Trans. 12A (1981) 1647.
[22] S.G. Addepalli, N.P. Magtoto, J.A. Kelber, Surf. Sci. 458 (2000) 123.
[23] D. Sondericker, F. Jona, P.M. Marcus, Phys. Rev. B 34 (1986) 6770.
[24] A.J. Bradley, A. Taylor, Proc. R. Soc. Lond. Ser. A 159 (1937) 56.
[25] A. Taylor, N.J. Doyle, J. Appl. Crystallogr. 5 (1972) 201.
[26] P.A. Korzhavyi, A.V. Ruban, A.Y. Lozovoy, Y.K. Vekilov, I.A. Abrikosov, B. Johansson, Phys. Rev. B 61 (2000) 6003.
[27] C.J. Smithells, in: E.A. Brandes, G. Brook (Eds.), Smithells Metals Reference Book, Butterworth, London, Boston, 1991, p. 13.